Journal of Alzheimer's Disease 54 (2016) 359–371
DOI 10.3233/JAD-160102
IOS Press



# Multimodal Classification of Mild Cognitive Impairment Based on Partial Least Squares

Pingyue Wang[a], Kewei Chen[b], Li Yao[a,c], Bin Hu[c], Xia Wu[a,c], Jiacai Zhang[c], Qing Ye[c] and Xiaojuan Guo[a,c,*], for the Alzheimer's Disease Neuroimaging Initiative[1]
[a]*National Key Laboratory of Cognitive Neuroscience and Learning, Beijing Normal University, Beijing, China*
[b]*Banner Alzheimer's Institute and Banner Good Samaritan PET Center, Phoenix, AZ, USA*
[c]*College of Information Science and Technology, Beijing Normal University, Beijing, China*

Handling Associate Editor: Ram Bishnoi

Accepted 7 June 2016

**Abstract**. In recent years, increasing attention has been given to the identification of the conversion of mild cognitive impairment (MCI) to Alzheimer's disease (AD). Brain neuroimaging techniques have been widely used to support the classification or prediction of MCI. The present study combined magnetic resonance imaging (MRI), $^{18}$F-fluorodeoxyglucose PET (FDG-PET), and $^{18}$F-florbetapir PET (florbetapir-PET) to discriminate MCI converters (MCI-c, individuals with MCI who convert to AD) from MCI non-converters (MCI-nc, individuals with MCI who have not converted to AD in the follow-up period) based on the partial least squares (PLS) method. Two types of PLS models (informed PLS and agnostic PLS) were built based on 64 MCI-c and 65 MCI-nc from the Alzheimer's Disease Neuroimaging Initiative (ADNI) database. The results showed that the three-modality informed PLS model achieved better classification accuracy of 81.40%, sensitivity of 79.69%, and specificity of 83.08% compared with the single-modality model, and the three-modality agnostic PLS model also achieved better classification compared with the two-modality model. Moreover, combining the three modalities with clinical test score (ADAS-cog), the agnostic PLS model (independent data: florbetapir-PET; dependent data: FDG-PET and MRI) achieved optimal accuracy of 86.05%, sensitivity of 81.25%, and specificity of 90.77%. In addition, the comparison of PLS, support vector machine (SVM), and random forest (RF) showed greater diagnostic power of PLS. These results suggested that our multimodal PLS model has the potential to discriminate MCI-c from the MCI-nc and may therefore be helpful in the early diagnosis of AD.

Keywords: Classification, mild cognitive impairment, MRI, partial least squares, PET

## INTRODUCTION

Alzheimer's disease (AD), a common form of dementia in the elderly, is a neurodegenerative disease accompanied by gray matter (GM) atrophy, hypometabolism, and amyloid-β (Aβ) deposition [1–3]. Mild cognitive impairment (MCI), as a transitional stage between normal aging and dementia, has attracted increasing attention from researchers [1, 4–9]. At this stage, patients have already presented some of the above-mentioned imaging changes [5, 6, 8, 10] but do not meet the criteria for AD [11–13]. However, some of the patients with MCI possibly

[1]Data used in preparation of this article were obtained from the Alzheimer's Disease Neuroimaging Initiative (ADNI) database (http://adni.loni.usc.edu). As such, the investigators within the ADNI contributed to the design and implementation of ADNI and/or provided data but did not participate in analysis or writing of this report. A complete listing of ADNI investigators can be found at: http://adni.loni.usc.edu/wp-content/uploads/how_to_apply/ADNI_Acknowledgement_List.pdf

*Correspondence to: Xiaojuan Guo, PhD, College of Information Science and Technology, Beijing Normal University, No. 19, XinJieKouWai St., HaiDian District, Beijing, China. Tel.: +86 10 58800427; Fax: +86 10 58800056; E-mail: gxj@bnu.edu.cn.

convert to AD in the near future, and the annual conversion rate is approximately 10% to 25% [14]. Therefore, studying MCI for the early detection of AD is extremely important.

Neuroimaging technologies, such as magnetic resonance imaging (MRI) and positron emission tomography (PET), have been widely used in the study of MCI and AD [4–7, 9, 10, 15–19]. MRI can be used to measure brain GM volume. $^{18}$F-fluorodeoxyglucose PET (FDG-PET) can evaluate the regional cerebral metabolic rate for glucose in the brain (CMRgl), and $^{18}$F-florbetapir PET (florbetapir-PET) can be applied to detect Aβ deposition [1, 3, 12]. Studies have shown that, relative to MCI non-converters (MCI-nc, individuals with MCI who have not converted to AD in the follow-up period) at baseline, MCI converters (MCI-c, individuals with MCI who convert to AD) have metabolic deficits in the left middle and superior temporal gyri [10], increased Aβ deposition in posterior medial and lateral cortical regions [20], and GM atrophy in the hippocampus, much of the temporal lobe, posterior cingulate gyrus, and precuneus [6, 18, 19]. The between-group differences in brain imaging data are extremely valuable for the classification of MCI-c and MCI-nc groups. However, the differences in single modality data are relatively subtle and may be not sufficient for improving classification performance. Recently, multimodal neuroimaging data have been used in a number of MCI studies that demonstrated that different modalities provide complementary information for MCI prediction or classification [9, 16, 18, 21–24]. Therefore, combining different modalities of neuroimaging data may be necessary for distinguishing MCI-c from MCI-nc.

Several classification methods have been used to categorize the MCI-c and MCI-nc groups based on multimodal imaging data and clinical test scores [9, 16, 18, 23, 24]. For example, Classification of Morphological Patterns Using Adaptive Regional Elements (COMPARE) was used to predict whether individuals with MCI will convert to AD, combining Spatial Pattern of Abnormalities for Recognition of Early AD (SPARE-AD) with cerebrospinal fluid (CSF) data [18]. Support vector machine (SVM) was used by Zhang et al. to classify MCI-c subjects from MCI-nc subjects based on MRI, PET and clinical test scores such as Mini-Mental State Examination (MMSE) and Alzheimer's Disease Assessment Scale-Cognitive Subscale (ADAS-Cog) [16]. Most of the reported multimodal classification methods were performed based on regions of interest (ROI). ROI-based methods allow for determining specific ROIs that contribute to the classification accuracy of diagnostic groups, and therefore show which ROIs are most biologically meaningful in the discrimination of MCI-c and MCI-nc. However, ROI-based methods require one to know the abnormal brain regions related to the disease in advance and are limited to some specific regions. Furthermore, the abnormal brain region may be a portion of one ROI or cover several ROIs, which may affect the performance of classifier [25]. Hinrichs et al. used Multi-Kernel Learning (MKL) to analyze MRI and FDG-PET data based on the voxel to generate Multi-Modality Disease Marker (MMDM) scores and applied the scores to predict the conversion from MCI to AD [24]. Liu et al. proposed a hierarchical ensemble classification method to make full use of the rich MRI imaging information, and improved the AD versus normal control classification result [25], which demonstrates the voxel-wise analysis method is useful in discrimination.

Partial least squares (PLS), a multivariate analysis technique with the advantages of principal component analysis (PCA) and multiple linear regression, can fully apply the voxel information from multimodal imaging data to prediction or classification [26, 27]. Moreover, PLS can extract the latent variable pairs from independent and dependent variables to overcome the problem of multiple correlation and possible noise in the large imaging data. Several studies have applied PLS as a classification tool for aging and dementia diagnosis [28–31]. For example, Chen et al. used multimodal PLS to separate older and younger subjects with an accuracy of 100% based on MRI and FDG-PET images, which illustrated the potential classification power of this method [30]. Therefore, it is worth while to examine the performance of the PLS method when combining multimodal imaging data with clinical test scores in the classification of MCI-c and MCI-nc based on the voxel across the whole brain.

In this study, we applied the PLS method to classify MCI-c from MCI-nc based on multimodal brain imaging data (florbetapir-PET, FDG-PET, and MRI) and clinical test score (ADAS-cog). According to the differences in design between the independent and dependent matrices, we built two types of PLS models (informed PLS and agnostic PLS) and examined their classification performances. In addition, we evaluated the diagnostic power of PLS in comparison with SVM and random forest (RF) methods respectively.

## MATERIALS AND METHODS

### *ADNI*

Data used in the preparation of this article were obtained from the Alzheimer's disease Neuroimaging Initiative (ADNI) database (http://adni.loni.usc.edu). The ADNI was launched in 2003 as a public-private partnership, led by Principal Investigator Michael W. Weiner, MD. The primary goal of ADNI has been to test whether serial MRI, PET, other biological markers, and clinical and neuropsychological assessment can be combined to measure the progression of MCI and early AD. For up-to-date information, see http://www.adni-info.org.

### *Participants*

The ADNI general inclusion criteria are described in detail at https://adni.loni.usc.edu/wp-content/uploads/2010/09/ADNI_GeneralProceduresManual.pdf. Enrolled subjects were between 55–90 years of age. According to the ADNI clinical inclusion criteria, for the diagnosis of MCI, the subjects showed subjective memory complaint and objective memory loss as measured by education-adjusted scores on Wechsler Memory Scale Logical Memory II, had MMSE scores between 24 and 30 and a clinical dementia rating (CDR) of 0.5. These individuals had general cognition and functional performance sufficiently preserved but with the absence of dementia.

This study included 129 subjects with MCI that were followed up for three years with all corresponding florbetapir-PET, FDG-PET, and MRI data at baseline. Within three years, 64 participants (MCI-c) converted to AD, while the other 65 participants (MCI-nc) maintained their MCI status. Table 1 lists the demographic information for all of these subjects. The MCI-c group did not significantly differ from the MCI-nc group in gender ($\chi^2_{(1)} = 0.37$, $p = 0.54$), age ($t_{(127)} = 0.304$, $p = 0.76$) or educational level ($t_{(127)} = 0.613$, $p = 0.54$) but had significantly more APOE $\varepsilon 4$ carriers ($\chi^2_{(2)} = 24.08$, $p = 5.92\text{e}-6$) and lower MMSE scores ($t_{(127)} = -4.46$, $p = 1.78\text{e}-5$) and higher ADAS-cog scores ($t_{(127)} = 9.47$, $p = 1.99\text{e}-16$). For each subject, the imaging time intervals of florbetapir-PET, FDG-PET and MRI were no more than three months.

Table 1
Demographic information for the subjects in this study

| | MCI-c ($n = 64$) | MCI-nc ($n = 65$) | $p$-value |
|---|---|---|---|
| Gender (female/male) | 29/35 | 26/39 | 0.54 |
| Age | $72.5 \pm 7.4$ | $72.2 \pm 7.5$ | 0.76 |
| Conv Time (years) | $1.4 \pm 0.7$ | – | – |
| Last follow-up time | – | $3.1 \pm 0.2$ | – |
| Years of education | $16.1 \pm 2.7$ | $15.8 \pm 2.4$ | 0.54 |
| APOE $\varepsilon 4$ (NC/HT/HM) | 15/37/12 | 43/18/4 | 5.92e-6 |
| MMSE | $26.9 \pm 1.9$ | $28.3 \pm 1.8$ | 1.78e-5 |
| ADAS-cog | $14.4 \pm 5.2$ | $7.4 \pm 2.9$ | 1.99e-16 |

MCI, mild cognitive impairment; MCI-c, MCI converter; MCI-nc, MCI non-converter; APOE, apolipoprotein E; NC, non-carrier; HT, heterozygote; HM, homozygote; MMSE, Mini-Mental State Examination; ADAS-cog, Alzheimer's Disease Assessment Scale-Cognitive Subscale; Conv Time, conversion time.

### *MRI data acquisition*

For each participant, T1-weighted image was obtained from 1.5T (15 subjects) or 3T (114 subjects) scanners. MRI data were acquired from various sites and platforms with somewhat different acquisition parameters. For each subject, sagittally oriented 3D anatomical image was collected using the MPRAGE sequence with $1.25 \times 1.25$ mm in-plane spatial resolution and 1.2-mm thickness. To enhance standardization across sites and platforms, each MRI dataset was preprocessed, which included gradwarp, B1 non-uniformity and N3 to correct gradient nonlinearity and intensity non-uniformity. Details regarding MRI Pre-processing can be found at http://adni.loni.usc.edu/methods/mri-analysis/mri-pre-processing/.

### *PET data acquisition*

A detailed description of PET protocols and acquisition can be found at http://www.adni-info.org. Briefly, PET images were acquired 30–60 min post-injection at a rate of one frame per 5 min. Then, raw PET images were processed to remove the possible differences resulting from using different scanners. For each subject, each frame was coregistered to the first frame, and then all frames were averaged to generate a single average image. The averaged image was reoriented and filtered into a standard $160 \times 160 \times 96$ voxel image grid having 1.5 mm cubic voxels. Finally, the images were smoothed with 8 mm FWHM Gaussian kernels. Details of the PET pre-processing were described at http://adni.loni.usc.edu/methods/pet-analysis/pre-processing/. The pre-processed PET images including steps of 'Co-reg, Avg, StdImg and VoxSiz, Uniform Resolution' were downloaded for the subsequent image preprocessing and statistical analysis.

*Image preprocessing*

All of the images were preprocessed in SPM8 (http://www.fil.ion.ucl.ac.uk/spm) based on MATLAB (Mathworks Inc., Sherborn, MA, USA) software. For each subject's MRI image, automated segmentation and normalization procedures [32–35] were performed in VBM8 Toolbox (http://dbm.neuro.uni-jena.de/vbm-8). GM maps were normalized by a protocol called diffeomorphic anatomical registration using exponential lie algebra (DARTEL) [32] into Montreal Neurological Institute (MNI) space. Finally, a common optimal GM mask was created with an optimal threshold using Masking toolbox (http://www.cs.ucl.ac.uk/staff/g.ridgway/masking) for extracting voxels in the subsequent section for creating numerical matrices. For each subject's PET images, first, florbetapir-PET and FDG-PET images were separately co-registered to the corresponding subject's MR images and then normalized to MNI space using the normalization parameters derived from MRI deformations. Then, each PET image was normalized to the average intensity of the reference region to generate the standardized uptake value ratio (SUVR) map. The global cerebrum was the reference region for FDG-PET images, while the cerebellum was the reference region for florbetapir-PET images [36]. Finally, all of the GM and SUVR maps were smoothed with 8 mm full width at half maximum (FWHM) Gaussian kernels.

*Creating data matrices*

Table 2 shows the independent datablock and dependent datablock in each specific PLS model. The independent block is referred to as $X$; the dependent block as $Y$. The single-modality informed PLS model uses $X_{florbetapir-PET}$, $X_{FDG-PET}$ and $X_{MRI}$ as independent blocks respectively. The imaging data matrix was created using voxels within the GM mask. For instance, for $X_{florbetapir-PET}$, we extracted voxel values within the GM mask from each SUVR map of florbetapir-PET and reshaped them as a row vector labelled as $v_1, v_2, \ldots, v_k$ (where k is the number of voxels within the GM mask, k = 295257 in this study). Then we stacked all row vectors as $X_{florbetapir-PET}$ by row. The row number is the number of subjects (129 in our study). Each column of $X_{florbetapir-PET}$ represents the corresponding voxel's value for each subject. The creating procedure of data $X_{FDG-PET}$ and $X_{MRI}$ matrices was similar to that of $X_{florbetapir-PET}$. The multi-modality informed PLS model used three imaging datasets florbetapir-PET, FDG-PET and MRI, stacked by column as independent blocks. In all informed models, MCI-c was designated as 1 and MCI-nc as 0 in the dependent block $Y$ to represent a subject's group membership. For agnostic PLS, we built six specific models: florbetapir–FDG, florbetapir–MRI, FDG–MRI, florbetapir–(FDG+MRI). FDG–(florbetapir+MRI) and MRI–(florbetapir+FDG). The agnostic PLS model is blind to group membership. Therefore, the independent block and dependent block were all designated as imaging data. For example, for the two-modality florbetapir—FDG model, the independent data is $X_{florbetapir-PET}$ and the dependent data is $X_{FDG-PET}$. The procedures of creating data matrices were similar to those of the informed PLS.

*Partial least squares analysis*

PLS analysis was performed by a MATLAB program written by Hervé Abdi [26] (http://www.utdallas.edu/ herve/). Briefly, PLS was performed according to the following steps:

Table 2
Independent datablocks and dependent datablocks for PLS models

| Model | $X$ | $Y$ |
|---|---|---|
| *Informed PLS model* | | |
| florbetapir | $[X_{florbetapir\text{-}PET}]$ | $[1,\ldots,1,0,\ldots,0]$ |
| FDG | $[X_{FDG\text{-}PET}]$ | $[1,\ldots,1,0,\ldots,0]$ |
| MRI | $[X_{MRI}]$ | $[1,\ldots,1,0,\ldots,0]$ |
| Combined | $[X_{MRI}, X_{FDG\text{-}PET}, X_{florbetapir\text{-}PET}]$ | $[1,\ldots,1,0,\ldots,0]$ |
| *Agnostic PLS model* | | |
| florbetapir–FDG | $[X_{florbetapir\text{-}PET}]$ | $[X_{FDG\text{-}PET}]$ |
| florbetapir–MRI | $[X_{florbetapir\text{-}PET}]$ | $[X_{MRI}]$ |
| FDG–MRI | $[X_{FDG\text{-}PET}]$ | $[X_{MRI}]$ |
| florbetapir–(FDG+MRI) | $[X_{florbetapir\text{-}PET}]$ | $[X_{FDG\text{-}PET}, X_{MRI}]$ |
| FDG–(florbetapir+MRI) | $[X_{FDG\text{-}PET}]$ | $[X_{florbetapir\text{-}PET}, X_{MRI}]$ |
| MRI–(florbetapir+FDG) | $[X_{MRI}]$ | $[X_{florbetapir\text{-}PET}, X_{FDG}]$ |

$X$ is the independent datablock, $Y$ is the dependent datablock.

1) The first latent variable of $X$ is $t = Xw$ where $w = (w_1, w_2, \ldots)'$ with norm $||w|| = 1$. Furthermore, $w_j$ is a scalar for variable $x_j$, which is the *jth* column of $X$ ($j = 1,\ 2 \ldots k$). Similarly, the first latent variable of $Y$ can be expressed as $u = Yc$ with norm $||c|| = 1$. $w$ and $c$ are calculated by maximizing the covariance between the latent variables. $w$ has been shown to be the corresponding eigenvector of matrix $\left[X'YY'X\right]$, and c has been shown to be that of matrix $\left[Y'XX'Y\right]$. $t$ and $u$ are called the first latent variable pair of $X$ and $Y$. When $w$ or $c$ represents weight coefficients of imaging voxels, it can be transformed into Z-scores and reshaped into 3D map that depicted covarying patterns of imaging data. A detailed description regarding constructing latent variables can be found at [30].
2) The contributions of the first latent variable are regressed out from $X$ and $Y$ to construct the new latent variable pair.
3) Steps 1 and 2 are repeated to construct the second latent variable pair, up to $L$, where $L = rank\,(X)$.
4) The predicted $Y$ can be expressed as $\hat{Y} = TBC^T = XB_{PLS}$, where $B_{PLS} = P^{T+}BC^T$ ($P^{T+}$ is the Moore-Penrose pseudo-inverse of $P^T$), $T$ is the matrix storing a set of latent variables that model $X$ and that simultaneously predict $Y$, $B$ is a diagonal matrix of slopes of the predictions of $Y$ from $T$, $C$ is the factor loadings of $Y$, and $P$ is the factor loadings of $X$.

*Leave-one-out cross-validation*

In informed PLS, we used the leave-one-out cross-validation method to obtain the PLS classification results. Briefly, the PLS procedure was repeated 129 times (the number of all subjects), leaving one subject out as a test sample each time. If the predicted group membership value for the test subject is closer to 1, then the predicted group is MCI-c, while if this value is closer to 0, then the predicted group is MCI-nc. Finally, we calculated the classification accuracy, sensitivity, and specificity.

*Fisher's linear discriminant analysis (Fisher's LDA)*

Fisher's LDA was implemented in SPSS 18.0 (SPSS, Inc., Chicago, IL, USA). In agnostic PLS, the extracted latent variables were input as variables of Fisher's LDA. The leave-one-out cross-validation method was applied to investigate the performance of the agnostic PLS model in classifying MCI-nc subjects from the MCI-c group. In addition, the classification effect of the clinical test score (ADAS-cog) was also evaluated in combination with the latent variables.

*Receiver operating curve (ROC) analysis*

We performed ROC analysis to obtain ROC curve and Area under the curve (AUC) to evaluate the performance of each PLS model with the numerical outcome of subsequently used classifiers of these PLS models. ROC analysis was implemented in SPSS 18.0.

*Support vector machine (SVM) and random forest (RF)*

SVM and RF were commonly used classification methods. In this study, we also used these two methods to classify MCI-c/MCI-nc and compared classification results with those of PLS. SVM is a pattern classification algorithm based on the structure risk minimization theory. RF is an ensemble classification model consisting of many decision trees, where the final predicted class label for the test samples decided by voting the predictions of all individual trees. We also built four models: florbetapir, FDG, MRI, Combined (combining three modalities) for SVM and RF respectively. The construction of the independent and dependent data matrices was the same to that of informed PLS. Leave-one-out cross-validation was also used to evaluate the classification performance. SVM was implemented by LIBSVM toolbox

(http://wwwcsientuedutw/vs.cjlin/libsvm) and the linear kernel function was used. RF was performed by Windows-Precompiled-RF_Mexstandalone-v0.02 toolbox

(https://randomforest-matlab.googlecode.com/files/Windows-Precompiled-RF_Mexstandalone-v0.02-.zip) and the number of trees was 500.

## RESULTS

*Classification of informed PLS models*

The number of latent variables was determined according to the optimal classification accuracy resulted from leave-one-out cross-validation method. In this way, the first three pairs of latent variables were

Table 3
Classification results for MCI-c versus MCI-nc based on informed PLS models

| Model | Accuracy (%) | Sensitivity (%) | Specificity (%) |
|---|---|---|---|
| florbetapir | 74.42 | 75.00 | 73.85 |
| FDG | 75.97 | 68.75 | 83.08 |
| MRI | 69.77 | 64.06 | 75.38 |
| Combined | 81.40 | 79.69 | 83.08 |

used for each informed PLS model. Table 3 shows the classification accuracy, sensitivity, and specificity of different informed PLS models. Specifically, results of three single-modality models differ: the best accuracy is 75.97% when using FDG-PET, and the lowest accuracy is 69.77% when MRI is used. Relative to all single-modality models, the multimodal informed model achieves better classification results (81.40% accuracy, 79.69% sensitivity, and 83.08% specificity) than any unimodal PLS model.

In addition, Fig. 1a shows the ROC curves of four models regarding the classification between MCI-c and MCI-nc. The greatest area under the ROC curve (AUC) is 0.856 for the multimodal model.

*Classification of agnostic PLS models*

The optimal number of latent variables was selected in the same way as that used in the informed PLS model. Table 4 shows the classification accuracy, sensitivity, and specificity results of different agnostic PLS models based on Fisher's LDA. The florbetapir–FDG and florbetapir–MRI model performs optimally (79.07% accuracy) among two-modality models. However, three-modality models outperform two-modality models. florbetapir–(FDG+MRI) achieves the best classification result (accuracy: 82.17%, sensitivity: 81.25% and specificity: 83.08%). ROC curves are shown in Fig. 1b. The greatest AUC is 0.907 for the florbetapir–(FDG+MRI) model. AUC of this model is significantly higher than the three-modality informed PLS model ($p = 0.024$).

We also evaluated the performance of ADAS-cog and MMSE for MCI-c versus MCI-nc classification based on Fisher's LDA. The ADAS-cog obtains better result (accuracy: 79.07%, sensitivity: 73.44% and specificity: 84.62%) than MMSE (accuracy: 67.44%, sensitivity: 60.94% and specificity: 73.85%). The classification results combining imaging data and ADAS-cog are improved (Table 4). In particular, the florbetapir–(FDG+MRI) model achieves an optimal classification accuracy of 86.05%, sensitivity of 81.25%, and specificity of 90.77%.

*Classification of SVM and RF*

Table 5 shows classification results of SVM and RF. For single-modality SVM, the highest accuracy is 75.19% for FDG-PET, and the lowest is 67.44% for MRI. However when combining all three imaging data, the result is the best (accuracy: 76.74%). For RF, the model of combining three modalities also obtains the best result (accuracy 73.64%). Figure 2 shows the histogram of results for informed PLS, SVM, and RF.

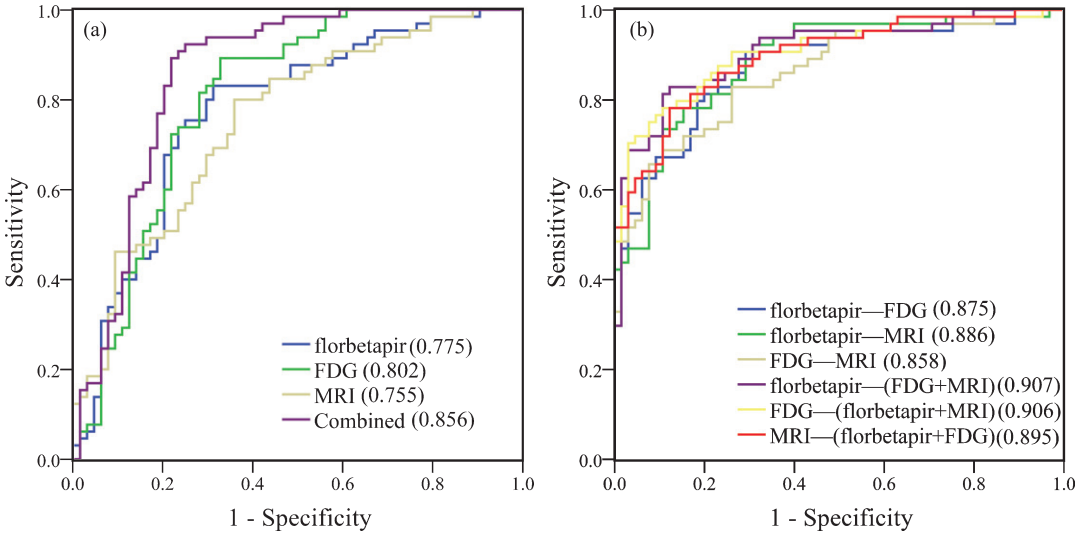


Fig. 1. ROC curves for MCI-c versus MCI-nc classification. (a) and (b) are curves of informed PLS and agnostic PLS based on neuroimaging data respectively. Numbers in parentheses are the AUCs.

Table 4
Classification results for MCI-c versus MCI-nc based on agnostic PLS models

| Model | Neuroimaging data | | | Neuroimaging data+ADAS-cog | | |
|---|---|---|---|---|---|---|
| | Accuracy (%) | Sensitivity (%) | Specificity (%) | Accuracy (%) | Sensitivity (%) | Specificity (%) |
| florbetapir–FDG | 79.07 | 79.69 | 78.46 | 83.72 | 78.13 | 89.23 |
| florbetapir–MRI | 79.07 | 79.69 | 78.46 | 83.72 | 84.38 | 83.08 |
| FDG–MRI | 74.42 | 70.31 | 78.46 | 84.50 | 82.81 | 86.15 |
| florbetapir–(FDG+MRI) | 82.17 | 81.25 | 83.08 | 86.05 | 81.25 | 90.77 |
| FDG–(florbetapir+MRI) | 79.84 | 78.13 | 81.54 | 84.50 | 79.69 | 89.23 |
| MRI–(florbetapir+FDG) | 79.07 | 81.25 | 76.92 | 84.50 | 79.69 | 89.23 |

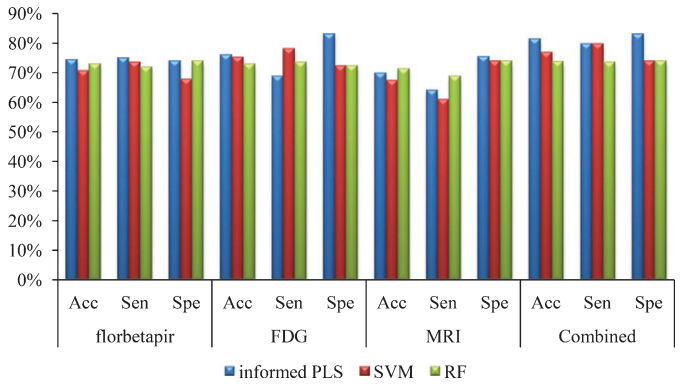


Fig. 2. Graph of prediction accuracy, sensitivity, and specificity based on informed PLS, SVM, and RF methods.

*Covarying patterns of three modalities*

Figure 3 shows the covarying patterns across florbetapir-PET, FDG-PET, and MRI generated by the multimodal informed PLS model (Fig. 3a) and the florbetapir–(FDG+MRI) agnostic PLS model (Fig. 3b) for the first latent variable. Colors represent Z-scores and are scaled to fit the range of each modality. For the multimodal informed PLS model, the MCI-related covarying brain regions mainly involved fusiform gyrus, middle/inferior temporal gyrus, middle/superior frontal gyrus and precuneus for florbetapir-PET; posterior cingulate cortex, precuneus, angular gyrus, inferior parietal lobule and inferior/middle temporal gyrus for FDG-PET; hippocampus, parahippocampus, amygdala and middle/inferior temporal gyrus for MRI. For the florbetapir–(FDG+MRI) agnostic PLS model, the MCI-related major brain regions involved in covarying patterns were similar to those of informed PLS model.

## DISCUSSION

In this study, PLS, a multimodal and multivariate data analysis technique, was used to combine three modalities of imaging data (florbetapir-PET, FDG-PET, and MRI) and clinical test score (ADAS-cog) to discriminate MCI-c subjects from the MCI-nc group. Two types of PLS models (informed PLS and agnostic PLS) were built, and the classification abilities of single-modality and multimodal PLS models were evaluated.

Individuals with MCI are considered at high-risk of conversion to AD [37]. The existing documents reported significant differences in GM volume, CMRgl, and Aβ deposition between MCI-c and MCI-nc groups [10, 18–20]. Therefore, MRI and PET data have been used widely in the classification of MCI in neuroimaging studies [4, 9, 16–18, 21, 38]. In this study, MRI and PET data were entered as the initial data matrices in two types of PLS models, informed PLS and agnostic PLS. The results showed that the three-modality informed PLS model achieved better classification accuracy compared with the single-modality model, and the three-modality agnostic PLS model also achieved better classification compared with the two-modality model. We noted that the results of both FDG–(florbetapir+MRI) and MRI–(florbetapir+FDG) agnostic models were inferior to that of florbetapir–(FDG+MRI) model, which suggested that the order of the different neuroimaging variables may affect the classification result. During the disease development of AD, Aβ

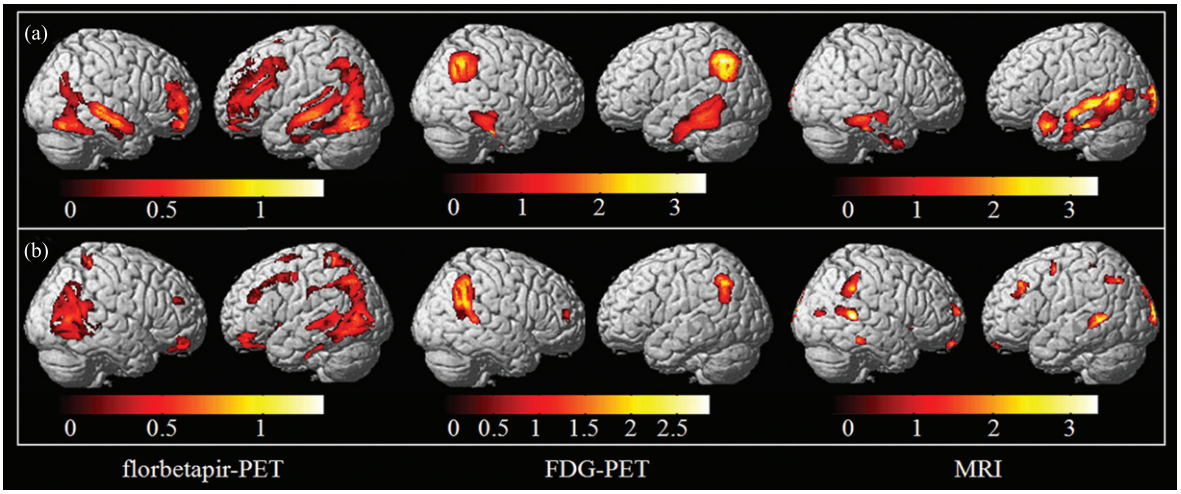


Fig. 3. The covarying patterns of florbetapir-PET, FDG-PET, and MRI for MCI-c versus MCI-nc classification for PLS models. (a): Combined informed PLS; (b): florbetapir–(FDG+MRI) agnostic PLS.

Table 5
Classification results for MCI-c versus MCI-nc based on SVM and RF methods

| Model | SVM | | | RF | | |
|---|---|---|---|---|---|---|
| | Accuracy (%) | Sensitivity (%) | Specificity (%) | Accuracy (%) | Sensitivity (%) | Specificity (%) |
| florbetapir | 70.54 | 73.44 | 67.69 | 72.87 | 71.88 | 73.85 |
| FDG | 75.19 | 78.12 | 72.31 | 72.87 | 73.44 | 72.31 |
| MRI | 67.44 | 60.94 | 73.85 | 71.32 | 68.75 | 73.85 |
| Combined | 76.74 | 79.69 | 73.85 | 73.64 | 73.44 | 73.85 |

SVM, Support Vector Machine; RF, Random Forest.

deposition appears earlier than gray matter atrophy and hypometabolism [3]. The optimal classification results of the model of florbetapir–(FDG+MRI) seemed to confirm this point implicitly. Additionally, the ROC analysis showed the three-modality agnostic model of florbetapir–(FDG+MRI) had higher statistical power than the three-modality informed PLS model ($p < 0.05$). The classification performance was further improved when neuroimaging data were combined with clinical test score (ADAS-cog) in the agnostic PLS model. Actually, in the informed PLS, the ADAS-cog was also combined with neuroimaging data (not shown). However the result did not change probably because the neruimaging data matrix was so large that the effect of clinical test score was submerged.

In addition, we applied SVM and RF methods to MCI-c versus MCI-nc discrimination respectively. Informed PLS outperformed these two methods especially when three modalities were fused. In order to make the results comparable, SVM and RF classifications were performed based on the voxel-wise data. Compared to SVM and RF, one of the advantages of PLS can address multiple correlations within and between modalities by extracting latent variables from imaging data.

Table 6 lists the classification results reported in literatures and our study. In the existing MCI classification studies, for example, Cho et al. used cortical thickness data extracted from MRI for unimodal classification to discriminate MCI-c subjects from MCI-nc groups (from ADNI) and obtained a sensitivity of 63% and specificity of 76% based on the incremental learning method [38], which was comparable with our result for the informed PLS model with MRI data only. Bakkour et al. predicted progression to mild AD with 83% sensitivity and 65% specificity based on ROC analysis using 29 Non-progressors and 20 Progressor from OASIS (Open Access Series of Imaging Studies) [39]. The sensitivity is higher than that of us but specificity is lower. More recently, Trzepacz et al. obtained accuracies of 62% and 66%, sensitivities of 10% and 45%, and specificities of 97% and 80% using FDG-PET and PIB-PET data, respectively, based on elastic net logistic regression of MCI-c and MCI-nc data from the ADNI database [9]. Our results for these two unimodal informed PLS models were better in term of

Table 6
Comparison of classification results reported in literatures and our study

| Articles | Modalties | Methods | Subjects | Accuracy (%) | Sensitivity (%) | Specificity (%) |
|---|---|---|---|---|---|---|
| Cho et al. [38] | MRI | Incremental learning | 131 MCI-nc+72 MCI-c (ADNI) | – | 63 | 76 |
| Bakkour et al. [39] | MRI | ROC | 29 Nonprogressors+20 Progressors (OASIS) | – | 83 | 65 |
| Trzepacz et al. [9] | FDG-PET | Elastic net logistic regression | 30 MCI-nc+20 MCI-c (ADNI) | 62 | 10 | 97 |
| | PIB-PET | | | 66 | 45 | 80 |
| | MRI | | | 67 | 37 | 87 |
| | MRI, PIB-PET | | | 76 | 53 | 90 |
| | MRI, FDG-PET | | | 69 | 37 | 90 |
| Westman et al. [40] | MRI | OPLS | 444 MCI (AddNeuroMed/ADNI) | – | 71 | 60 |
| Gray et al. [42] | FDG-PET, MRI | Random forest | 34 pMCI+41 sMCI (ADNI) | 58.0 | 57.1 | 58.7 |
| Teipel et al. [20] | AV45-PET, FDG-PET, MRI | Logistic regression | 88 MCI-nc+39 MCI-c (ADNI) | 72 | – | – |
| Zhang et al. [16] | MRI | SVM+ROC | 50 MCI-nc+38 MCI-c (ADNI) | 0.697 (AUC) | – | – |
| | MRI, FDG-PET, MMSE, ADAS-cog | | | 0.768 (AUC) | – | – |
| Cui et al. [43] | MRI | SVM | 153 Non-decliners+33 decliners (MAS) | 63.80 | 64.17 | 63.79 |
| | MRI, NMs | | | 78.51 | 73.33 | 79.75 |
| Our study | florbetapir-PET, FDG-PET, MRI, ADAS-cog | Agnostic PLS | 64 MCI-c+65 MCI-nc (ADNI) | 86.05 | 81.25 | 90.77 |

NMs, neuropsychological measures; MKL, multi-kernel learning; OASIS, Open Access Series of Imaging Studies; AUC, the corresponding area under the ROC curve; MAS, Sydney Memory and Ageing Study; SVM, Support Vector Machine.

accuracy than those of Trzepacz et al. However, in contrast with our results, in [9], MRI had the highest and FDG had the lowest accuracy. In addition, Westman et al. applied orthogonal partial least squares (OPLS) in MRI data to predict conversion from MCI to AD, resulting in a sensitivity of 71% better than our result when only using MRI data [40]. The potential reasons for the discrepancy may be the different methodologies and features employed.

Recently, several studies have combined multimodal neuroimaging data in MCI classification or prediction studies [9, 16, 18, 23, 24, 41, 42]. For example, also Trzepacz et al. obtained an accuracy of 76%, sensitivity of 53% and specificity of 90% when MRI and PIB-PET data were fused [9]; the sensitivity and specificity of these results were not so balanced compared to our results when we used MRI and florbetapir-PET simultaneously in the agnostic PLS model. Balanced measurements would be more appropriate in predicting conversion of AD among MCI patients. This might be important as the accumulative conversion rate approximately 10% to 25% annually. MRI and FDG-PET were also combined in their study and achieved an accuracy of 69%, sensitivity of 37% and specificity of 90% [9]. Gray et al. also combined FDG-PET and MRI from ADNI based on random forest method for pMCI/sMCI classification, and achieved accuracy: 58.0%, sensitivity: 57.1%, and specificity: 58.7% [42]. These results were not superior to our result when these two modalities were combined. Until now, few MCI classification studies have combined MRI, florbetapir-PET, and FDG-PET. Compared with our three modalities results, Teipel et al. achieved 72% cross-validated accuracy for prediction of conversion status based on logistic regression models fusing those three modalities also from ADNI [20]. Furthermore, for both the informed PLS model and agnostic PLS model, three-modality models obtained better identification results compared to the single-modality and two-modality models. These results demonstrate that different neuroimaging modalities may provide complementary information that may be useful for increasing the accuracy of MCI classification.

Many studies have also examined the contribution of clinical test scores to discrimination [16, 23, 41, 43]. For example, Zhang et al. reported that the

accuracy, sensitivity, and specificity of discrimination were much improved when cognitive scores (MMSE and ADAS-cog) were combined based on the SVM method; the corresponding AUC values improved to 0.768 from 0.697 (0.697 is the AUC of the MRI-based dataset, which is the largest in the single modality method) [16]. Cui et al. also obtained better classification performance when combining MRI and neuropsychological measures for MCI prediction based on SVM [43]. In this study, we also examined the effect of clinical test score on the classification of MCI-nc and MCI-c groups. The ADAS-cog and MMSE were also used for classification based on Fisher's LDA. For the MMSE performs not well, we focus on the ADAS-cog only in this study. Our result presented the same trend in the agnostic PLS model as the previous study. Although, for informed PLS models, combining neuroimaging data with the ADAS-cog, the classification result was not improved for the effect of the ADAS-cog was potentially drowned in the large independent matrix. However, in the agnostic PLS model, the classification was completed by Fisher's LDA with the extracted latent variables and ADAS-cog as input variables. The effect of ADAS-cog was obvious. Accuracy, sensitivity and specificity were greatly improved (see Table 4), which indicates that the fusion of neuroimaging data and clinical test score can consistently and substantially optimize the classification results. Thus, ADAS-cog is a valuable measure for the detection of MCI-c relative to MCI-nc.

The maps of weight information of the imaging voxel represent the spatial covariation patterns classifying MCI-c from MCI-nc within or across modalities. The major brain regions involved in covarying patterns of informed PLS and agnostic PLS were similar in our study. These findings are similar to what reported in the univariate or unimodal studies with some differences [10, 20, 18], however, reflecting possible covarying patterns in this multimodal approach that are not observable otherwise.

PLS is a tool with potential value in the classification researches [30, 31]. The PLS method covers and generalizes the characteristics of PCA and multiple regression and is very useful, particularly when predicting the dependent variable dataset from a large number of independent variable dataset is required [26]. The prediction is completed by extracting a set of latent variables from dependent and independent variables, which have the best predictive power (maximizing the covariance between the linear combination of dependent and independent variables). The most obvious advantage of the PLS method is that it can be used to analyze neuroimaging data without prior information based on all voxels with multiple datablocks as dependent and independent variables. In this study, PLS was used to detect the progression of MCI. The informed PLS model incorporates the known information (group membership) regarding the variable of interest; however, the agnostic PLS model is blind to the membership information. The informed PLS model can be considered a classifier because it can complete classification by itself through predicting the group membership from neuroimaging data. After leave-one-out cross-validation procedure, we can calculate the accuracy, sensitivity, and specificity according to the predicted group membership. However, the agnostic PLS model cannot complete classification independently because the independent and dependent variables are all imaging data. Thus, we used Fisher's LDA to analyze the latent variables extracted by agnostic PLS. In addition, in the informed PLS model, the independent datablock was a neuroimaging data matrix; therefore, the effect of ADAS-cog could easily be obscured. However, for the agnostic PLS model, the classification was estimated by Fisher's LDA with the extracted latent variables as input variables. Therefore, the agnostic PLS model could improve results when combining ADAS-cog. Additionally, we tested the effect of different smoothing level (0 mm, 4 mm, 8 mm) of the SUVR maps on the classification results. The results showed the smoothing level had no significant influences on the accuracy, sensitivity, and specificity of four informed PLS models.

Our current study has some limitations. Firstly, the sample size is relatively small, which may lead to lower statistical power of classification. Our study was performed based on multimodality neuroimaging data; therefore, requiring each subject to have all of the corresponding modality data. This requirement limited the number of subjects available for our study. However, we used the leave-one-out cross-valid method to improve the reliability of the results and to reduce the possible influence of small sample size. Secondly, we only used the baseline data of each subject that was followed for three years. Longitudinal data may perform better in the analysis, and this possibility needs to be explored in future studies. Finally, the PLS method has the potential to combine additional modalities of imaging data.

Therefore, functional MRI and diffusion tensor imaging will be combined in future studies.

## CONCLUSION

In this study, we classified MCI-c subjects from MCI-nc subjects based on the PLS method and demonstrated that the multimodal PLS model outperformed the unimodal PLS model. We combined three modalities of neuroimaging data (florbetapir-PET, FDG-PET, and MRI) and clinical test score (ADAS-cog) and achieved valuable classification results. Furthermore, PLS showed greater diagnostic power compared with SVM and RF. In summary, our PLS models applied to identify the conversion of MCI to AD may be helpful for detecting MCI or for predicting AD. These models may also be useful in clinical diagnosis and pathological research.

## ACKNOWLEDGMENTS

This work was supported by the National Natural Science Foundation (NNSF), China (81000603), the Funds for International Cooperation and Exchange of NNSF, China (61210001), Key Program of NNSF, China (91320201), the Fundamental Research Funds for the Central Universities, China, the National Institute of Mental Health, US (RO1 MH57899), the National Institute on Aging, US (9R01AG031581-10, P30 AG19610), and the State of Arizona.

Data collection and sharing for this project was funded by the Alzheimer's Disease Neuroimaging Initiative (ADNI) (National Institutes of Health Grant U01 AG024904) and DOD ADNI (Department of Defense award number W81XWH-12-2-0012). ADNI is funded by the National Institute on Aging, the National Institute of Biomedical Imaging and Bioengineering, and through generous contributions from the following: AbbVie, Alzheimer's Association; Alzheimer's Drug Discovery Foundation; Araclon Biotech; BioClinica, Inc.; Biogen; Bristol-Myers Squibb Company; CereSpir, Inc.; Eisai Inc.; Elan Pharmaceuticals, Inc.; Eli Lilly and Company; EuroImmun; F. Hoffmann-La Roche Ltd and its affiliated company Genentech, Inc.; Fujirebio; GE Healthcare; IXICO Ltd.; Janssen Alzheimer Immunotherapy Research & Development, LLC.; Johnson & Johnson Pharmaceutical Research & Development LLC.; Lumosity; Lundbeck; Merck & Co., Inc.; Meso Scale Diagnostics, LLC.; NeuroRx Research; Neurotrack Technologies; Novartis Pharmaceuticals Corporation; Pfizer Inc.; Piramal Imaging; Servier; Takeda Pharmaceutical Company; and Transition Therapeutics. The Canadian Institutes of Health Research is providing funds to support ADNI clinical sites in Canada. Private sector contributions are facilitated by the Foundation for the National Institutes of Health (http://www.fnih.org). The grantee organization is the Northern California Institute for Research and Education, and the study is coordinated by the Alzheimer's Disease Cooperative Study at the University of California, San Diego. ADNI data are disseminated by the Laboratory for NeuroImaging at the University of Southern California.

Authors' disclosures available online (http://j-alz.com/manuscript-disclosures/16-0102r1).

## REFERENCES

[1] Braskie MN, Toga AW, Thompson PM (2012) Recent advances in imaging Alzheimer's disease. *J Alzheimers Dis* **33**, S313-S327.

[2] Frisoni GB, Fox NC, Jack CR, Scheltens P, Thompson PM (2010) The clinical use of structural MRI in Alzheimer disease. *Nat Rev Neurol* **6**, 67-77.

[3] Jack CR, Knopman DS, Jagust WJ, Petersen RC, Weiner MW, Aisen PS, Shaw LM, Vemuri P, Wiste HJ, Weigand SD (2013) Tracking pathophysiological processes in Alzheimer's disease: An updated hypothetical model of dynamic biomarkers. *Lancet Neurol* **12**, 207-216.

[4] Willette AA, Calhoun VD, Egan JM, Kapogiannis D (2014) Prognostic classification of mild cognitive impairment and Alzheimer's disease: MRI independent component analysis. *Psychiatry Res* **224**, 81-88.

[5] Karas G, Scheltens P, Rombouts S, Visser P, Van Schijndel R, Fox N, Barkhof F (2004) Global and local gray matter loss in mild cognitive impairment and Alzheimer's disease. *Neuroimage* **23**, 708-716.

[6] Misra C, Fan Y, Davatzikos C (2009) Baseline and longitudinal patterns of brain atrophy in MCI patients, and their use in prediction of short-term conversion to AD: Results from ADNI. *Neuroimage* **44**, 1415-1422.

[7] Leung KK, Shen K-K, Barnes J, Ridgway GR, Clarkson MJ, Fripp J, Salvado O, Meriaudeau F, Fox NC, Bourgeat P (2010) Increasing power to predict mild cognitive impairment conversion to Alzheimer's disease using hippocampal atrophy rate and statistical shape models. *In Medical Image Computing and Computer-Assisted Intervention–MICCAI 2010*, Springer, pp. 125-132.

[8] Pennanen C, Testa C, Laakso MP, Hallikainen M, Helkala EL, Hanninen T, Kivipelto M, Kononen M, Nissinen A, Tervo S, Vanhanen M, Vanninen R, Frisoni GB, Soininen H (2005) A voxel based morphometry study on mild cognitive impairment. *J Neurol Neurosurg Psychiatry* **76**, 11-14.

[9] Trzepacz PT, Yu P, Sun J, Schuh K, Case M, Witte MM, Hochstetler H, Hake A (2014) Comparison of neuroimag-

ing modalities for the prediction of conversion from mild cognitive impairment to Alzheimer's dementia. *Neurobiol Aging* **35**, 143-151.

[10] Morbelli S, Piccardo A, Villavecchia G, Dessi B, Brugnolo A, Piccini A, Caroli A, Frisoni G, Rodriguez G, Nobili F (2010) Mapping brain morphological and functional conversion patterns in amnestic MCI: A voxel-based MRI and FDG-PET study. *Eur J Nucl Med Mol Imaging* **37**, 36-45.

[11] Albert MS, DeKosky ST, Dickson D, Dubois B, Feldman HH, Fox NC, Gamst A, Holtzman DM, Jagust WJ, Petersen RC (2011) The diagnosis of mild cognitive impairment due to Alzheimer's disease: Recommendations from the National Institute on Aging-Alzheimer's Association workgroups on diagnostic guidelines for Alzheimer's disease. *Alzheimers Dement* **7**, 270-279.

[12] Dubois B, Feldman HH, Jacova C, Cummings JL, Dekosky ST, Barberger-Gateau P, Delacourte A, Frisoni G, Fox NC, Galasko D (2010) Revising the definition of Alzheimer's disease: A new lexicon. *Lancet Neurol* **9**, 1118-1127.

[13] Dubois B, Feldman HH, Jacova C, Hampel H, Molinuevo JL, Blennow K, DeKosky ST, Gauthier S, Selkoe D, Bateman R (2014) Advancing research diagnostic criteria for Alzheimer's disease: The IWG-2 criteria. *Lancet Neurol* **13**, 614-629.

[14] Grand JH, Caspar S, MacDonald SW (2011) Clinical features and multidisciplinary approaches to dementia care. *J Multidiscip Healthc* **4**, 125-147.

[15] Stonnington CM, Chu C, Klöppel S, Jack CR, Ashburner J, Frackowiak RS (2010) Predicting clinical scores from magnetic resonance scans in Alzheimer's disease. *Neuroimage* **51**, 1405-1413.

[16] Zhang D, Shen D (2012) Predicting future clinical changes of MCI patients using longitudinal and multimodal biomarkers. *PLoS One* **7**, e33182.

[17] Zhang D, Wang Y, Zhou L, Yuan H, Shen D (2011) Multimodal classification of Alzheimer's disease and mild cognitive impairment. *Neuroimage* **55**, 856-867.

[18] Davatzikos C, Bhatt P, Shaw LM, Batmanghelich KN, Trojanowski JQ (2011) Prediction of MCI to AD conversion, via MRI, CSF biomarkers, and pattern classification. *Neurobiol Aging* **32**, 2322.e19-2322.e27.

[19] Chetelat G, Landeau B, Eustache F, Mezenge F, Viader F, de La Sayette V, Desgranges B, Baron J-C (2005) Using voxel-based morphometry to map the structural changes associated with rapid conversion in MCI: A longitudinal MRI study. *Neuroimage* **27**, 934-946.

[20] Teipel SJ, Kurth J, Krause B, Grothe MJ (2015) The relative importance of imaging markers for the prediction of Alzheimer's disease dementia in mild cognitive impairment—Beyond classical regression. *Neuroimage Clin* **8**, 583-593.

[21] Walhovd K, Fjell A, Brewer J, McEvoy L, Fennema-Notestine C, Hagler D, Jennings R, Karow D, Dale A (2010) Combining MR imaging, positron-emission tomography, and CSF biomarkers in the diagnosis and prognosis of Alzheimer disease. *AJNR Am J Neuroradiol* **31**, 347-354.

[22] Fan Y, Resnick SM, Wu X, Davatzikos C (2008) Structural and functional biomarkers of prodromal Alzheimer's disease: A high-dimensional pattern classification study. *Neuroimage* **41**, 277-285.

[23] Cui Y, Liu B, Luo S, Zhen X, Fan M, Liu T, Zhu W, Park M, Jiang T, Jin JS (2011) Identification of conversion from mild cognitive impairment to Alzheimer's disease using multivariate predictors. *PLoS One* **6**, e21896.

[24] Hinrichs C, Singh V, Xu G, Johnson SC (2011) Predictive markers for AD in a multi-modality framework: An analysis of MCI progression in the ADNI population. *Neuroimage* **55**, 574-589.

[25] Liu M, Zhang D, Shen D (2014) Hierarchical fusion of features and classifier decisions for Alzheimer's disease diagnosis. *Hum Brain Mapp* **35**, 1305-1319.

[26] Abdi H (2010) Partial least squares regression and projection on latent structure regression (PLS Regression). *Wiley Interdiscip Rev Comput Stat* **2**, 97-106.

[27] Krishnan A, Williams LJ, Mcintosh AR, Abdi H (2011) Partial Least Squares (PLS) methods for neuroimaging: A tutorial and review. *Neuroimage* **56**, 455-475.

[28] Lehmann C, Koenig T, Jelic V, Prichep L, John RE, Wahlund L-O, Dodge Y, Dierks T (2007) Application and comparison of classification algorithms for recognition of Alzheimer's disease in electrical brain activity (EEG). *J Neurosci Methods* **161**, 342-350.

[29] Gottfries J, Blennow K, Wallin A, Gottfries C (1995) Diagnosis of dementias using partial least squares discriminant analysis. *Dement Geriatr Cogn Disord* **6**, 83-88.

[30] Chen K, Reiman EM, Huan Z, Caselli RJ, Bandy D, Ayutyanont N, Alexander GE (2009) Linking functional and structural brain images with multivariate network analyses: A novel application of the partial least square method. *Neuroimage* **47**, 602-610.

[31] Chen K, Ayutyanont N, Langbaum JB, Fleisher AS, Reschke C, Lee W, Liu X, Alexander GE, Bandy D, Caselli RJ (2012) Correlations between FDG PET glucose uptake-MRI gray matter volume scores and apolipoprotein E $\varepsilon 4$ gene dose in cognitively normal adults: A cross-validation study using voxel-based multi-modal partial least squares. *Neuroimage* **60**, 2316-2322.

[32] Ashburner J (2007) A fast diffeomorphic image registration algorithm. *Neuroimage* **38**, 95-113.

[33] Ashburner J, Friston KJ (2000) Voxel-based morphometry—the methods. *Neuroimage* **11**, 805-821.

[34] Rajapakse JC, Giedd JN, Rapoport JL (1997) Statistical approach to segmentation of single-channel cerebral MR images. *IEEE Trans Med Imaging* **16**, 176-186.

[35] Good CD, Johnsrude IS, Ashburner J, Henson RNA, Friston KJ, Frackowiak RSJ (2001) A voxel-based morphometric study of ageing in 465 normal adult human brains. *Neuroimage* **14**, 21-36.

[36] Jagust WJ, Landau SM, Koeppe RA, Reiman EM, Chen K, Mathis CA, Price JC, Foster NL, Wang AY (2015) The Alzheimer's Disease Neuroimaging Initiative 2 PET Core: 2015. *Alzheimers Dement* **11**, 757-771.

[37] Bruno D, Albert M (2004) Amnestic MCI or prodromal Alzheimer's disease? *Lancet Neurol* **3**, 246-248.

[38] Cho Y, Seong JK, Jeong Y, Shin SY (2012) Individual subject classification for Alzheimer's disease based on incremental learning using a spatial frequency representation of cortical thickness data. *Neuroimage* **59**, 2217-2230.

[39] Bakkour A, Morris J, Dickerson BC (2009) The cortical signature of prodromal AD Regional thinning predicts mild AD dementia. *Neurology* **72**, 1048-1055.

[40] Westman E, Simmons A, Muehlboeck J-S, Mecocci P, Vellas B, Tsolaki M, Kłoszewska I, Soininen H, Weiner

MW, Lovestone S (2011) AddNeuroMed and ADNI: Similar patterns of Alzheimer's atrophy and automated MRI classification accuracy in Europe and North America. *Neuroimage* **58**, 818-828.

[41] Ewers M, Walsh C, Trojanowski JQ, Shaw LM, Petersen RC, Jack CR, Feldman HH, Bokde AL, Alexander GE, Scheltens P (2012) Prediction of conversion from mild cognitive impairment to Alzheimer's disease dementia based upon biomarkers and neuropsychological test performance. *Neurobiol Aging* **33**, 1203-1214.

[42] Gray KR, Aljabar P, Heckemann RA, Hammers A, Rueckert D (2012) Random forest-based similarity measures for multi-modal classification of Alzheimer's disease. *Neuroimage* **65**, 167-175.

[43] Cui Y, Sachdev PS, Lipnicki DM, Jin JS, Luo S, Zhu W, Kochan NA, Reppermund S, Liu T, Trollor JN (2012) Predicting the development of mild cognitive impairment: A new use of pattern recognition. *Neuroimage* **60**, 894-901.